Powder Technology 436 (2024) 119510

Contents lists available at ScienceDirect

Powder Technology

journal homepage: www.journals.elsevier.com/powder-technology

Bi-metallic Ni–Fe LSF perovskite for chemical looping hydrogen application

Adam Zaidi, Christopher de Leeuwe, Vincenzo Spallina *

Department of Chemical Engineering, University of Manchester, Manchester M13 9PL, UK

HIGHLIGHTS

- Fe-based and LSF successfully tested at 900 °C for up to 20 consecutive cycles.
- 5 g of material was synthesised using wet impregnation and Pechini methods.
- Fe-based oxygen carrier capacity is lost after 10 redox cycles.
- LSF oxygen carrier capacity lost is limited to 16% after 70 h.
- 2.36 × 10^{-4} molH₂ per mol of oxygen carriers were recorded with no structural changes on LSF.

GRAPHICAL ABSTRACT

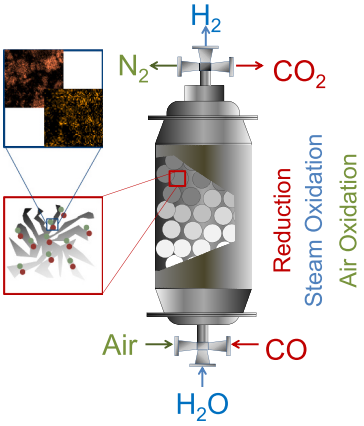

ARTICLE INFO

Keywords:
LSF
Chemical looping hydrogen
CO_2 capture
Oxygen carrier synthesis

ABSTRACT

This work introduces a novel composite bimetallic perovskite Fe_2O_3-NiO/$La_{0.6}Sr_{0.4}FeO_3$ as an oxygen carrier for chemical looping hydrogen production. The materials were tested in a

2-g packed bed reactor at different temperatures ranging from 500 to 900 °C and atmospheric pressure by alternating three-stage chemical looping hydrogen reactions. Fe—Ni bimetallic interactions and $La_{0.6}Sr_{0.4}FeO_3$ (LSF-641) resistance to carbon deposition resulted in a stable material with only a 2% oxygen capacity drop over 20 redox cycles. The modified LSF exhibited a 20 increase in H_2 generation compared to LSF-641. These results demonstrate the effectiveness of doping Fe with Ni to generate more stable OC and the low H_2 generation of LSF coupled with its greater redox cycling. Pre- and post-experimental (SEM-EDX) characteristics showed a homogenous distribution of Ni and Fe on the surface, thus confirming high stability to metal oxide cluster formation or sign of sintering.

1. Introduction

Hydrogen production accounts for 880 $MtCO_2$ emissions annually, with projections predicting over 1000 $MtCO_2$ emissions by 2025 [1]. While chemical looping has been widely presented in the literature [2,3], chemical looping hydrogen (CLH) production combines chemical looping processes and thermochemical water splitting in which H_2 from

* Corresponding author.
E-mail address: vincenzo.spallina@manchester.ac.uk (V. Spallina).

https://doi.org/10.1016/j.powtec.2024.119510
Received 9 November 2023; Received in revised form 8 January 2024; Accepted 4 February 2024
Available online 6 February 2024

Nomenclature

CL	chemical looping
CLR	chemical looping reforming
CLH	Chemical looping hydrogen
CLWS	chemical looping water splitting
OC	oxygen carrier
OTC	oxygen transport capacities
ROC	Rate of oxygen transport capacity
SEM-EDX	Scanning Electron with Energy Dispersive X-Ray Analysis
SIP	The steam iron process
SMR	Steam methane reforming
SSR	Solid-state synthesis
TGA	Thermal Gravimetric Analyser
XRD	X-ray diffraction

water reduction is generated. At the same time, inherent CO_2 is concentrated and separated. It occurs in a three-stage cyclic process (Fig. 1). The three-reactor set-up is advantageous for pure H_2 production due to the ability to generate separate streams of H_2, N_2 and CO_2. In addition, such configuration is thermally balanced, especially in the presence of fuel which contains CH_4 or other light hydrocarbons.

Chemical looping processes have utilised varying materials depending on the desired product, such as Ni-based oxygen carriers for syngas generation from glycerol in chemical looping reforming [4,5].Fe oxide is a well-known material for water splitting because the Fe_3O_4/FeO/Fe system has favourable phase change, leading to high steam-to-hydrogen conversion [6]. The reaction pathway is to oxidise Fe to Fe_3O_4 with H_2O or Fe_2O_3 with oxygen from the air. This is carried out via the following reactions via single or multi-step responses (1)-(5) [7]. Moreover, Fe-based OCs are also low cost, environmentally compatible, resistant to sulphur poisoning, non-toxic, have good mechanical strength, and have high oxygen storage capacity [8].

$$0.35Fe + H_2O \rightarrow 0.25Fe_3O_4 + H_2 \quad \Delta H_{298} = -38.3\ kJ/mol_{H_2O} \tag{1}$$

$$3FeO + H_2O \rightarrow Fe_3O_4 + H_2 \quad \Delta H_{298} = -74.7\ kJ/mol_{H_2O} \tag{2}$$

$$4/3Fe + O_2 \rightarrow 2/3Fe_2O_3 \quad \Delta H_{298} = -543.5\ kJ/mol_{O_2} \tag{3}$$

$$4FeO + O_2 \rightarrow 2Fe_2O_3 \quad \Delta H_{298} = -194.1\ kJ/mol_{O_2} \tag{4}$$

$$4Fe_3O_4 + O_2 \rightarrow 6Fe_2O_3 \quad \Delta H_{298} = -471.6\ kJ/mol_{O_2} \tag{5}$$

Complete reduction to metallic Fe increases the risk of sintering, leading to a loss in the OC performance [9]. Fe-based oxygen carriers are well known to work as oxygen carriers for CH_4 oxidation [10,11]. To improve stability, the addition of Ni, creating nickel ferrite species ($NiFe_2O_4$), has been considered to convert hydrocarbons such as toluene [12] or chemical looping combustion applications [12–14]. In chemical looping water splitting application, $NiFe_2O_4$ has shown good cyclability, with an increase in H_2 generation four-fold compared to Fe_2O_3 materials used in chemical looping processes.

A different family of suitable OC for CLH is the perovskite family, which has enhanced redox properties, high oxygen mobility, thermal stability, and resistance to carbon deposition. Zhu et al. [15] have presented a comprehensive study to unravel new material designs for chemical looping by tuning oxygen carrier properties for each specific reaction. Galvita et al. [16] confirmed the hypothesis of using perovskite for CO_2 to CO utilisation; Wang et al. [17] presented the advantage of doping $LaMnO_3$ with Fe to increase the production of syngas and H_2 within the same process. Sastre et al. [18] tested Ni-doped perovskite for CH_4 dry reforming to manipulate the H_2/CO ratio of the syngas generated.

$La_{0.6}Sr_{0.4}FeO_{3-\delta}$ (LSF-641) is a non-stoichiometric OC that shows stability over a wide range of partial pressure of oxygen, P_{O_2}, and high resistance to carbon deposition, which is well documented in the with De Leeuwe et al. [19] showing constant capacity over 1000 cycles, utilising water gas shift feed (CO as the fuel for reduction and H_2O for oxidation), offering 95% H_2O conversion at 1073 K compared to 50% of conventional water gas shift reactors operated at ≈470 K, resistance to carbon deposition, and enhanced kinetics due to the higher operating temperature, allowing for faster reaction rates and smaller reactors [20].

The issue with using Perovskites compared to transition metal-OC is that perovskites have lower oxygen transport capacities (OTC) than metallic OCs and lower surface area for reaction with the gas phase, limiting the H_2 generation [21]. To increase OTC, utilising the perovskite as an active support in composite oxides utilises the transition metal's high oxygen capacity and perovskite oxygen transport properties, rather than an inert such as Al_2O_3. Fe_2O_3 is an attractive transition metal to use in composite oxides, Fe_2O_3-LSF, due to its ability to split water into pure H_2 and the relative abundance and low cost of the material [22]. Galinsky et al. [23] conducted testing in a Thermal Gravimetric Analyser (TGA) of 60 wt% Fe_2O_3 supported on LSF-821, showed good stability and coke resistance, as well as an enhanced reactivity of 5–70 times with reducing gas feeds (H_2, CO and CH_4) compared with using inert material supported. He et al. [24] investigated using a TGA partial oxidation of 25% and 40% Fe_3O_4 supported on LSF-821. It showed a 15% greater steam conversion than predicted by the second law for unpromoted iron oxides, reducing the energy penalty on the process as the latent heat in the steam-H_2 outlet mixture cannot be fully

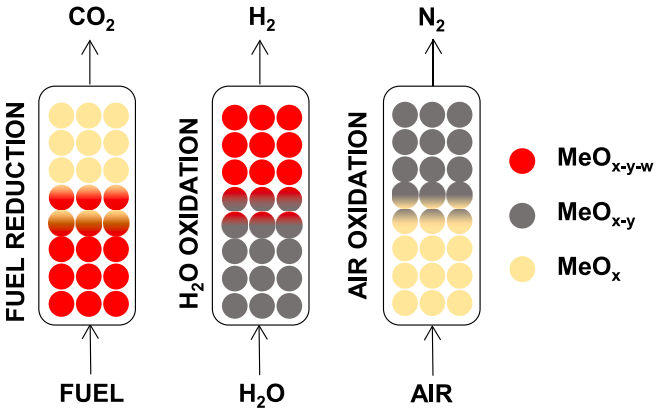

Fig. 1. Chemical looping hydrogen production stages in three-stage reactor configuration schematic.

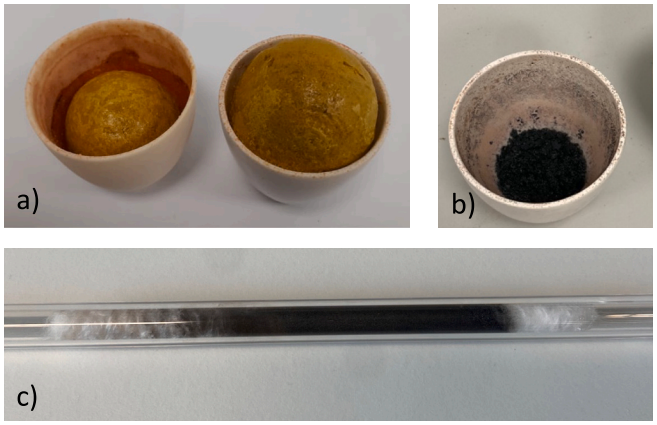

Fig. 2. Images showing $La_{0.6}Sr_{0.4}FeO_{3-\delta}$ synthesis. a) after the first heating stage; b) after the second heating stage; c) quartz-packed bed reactors, showing packing of $La_{0.6}Sr_{0.4}FeO_{3-\delta}$ used for the testing.

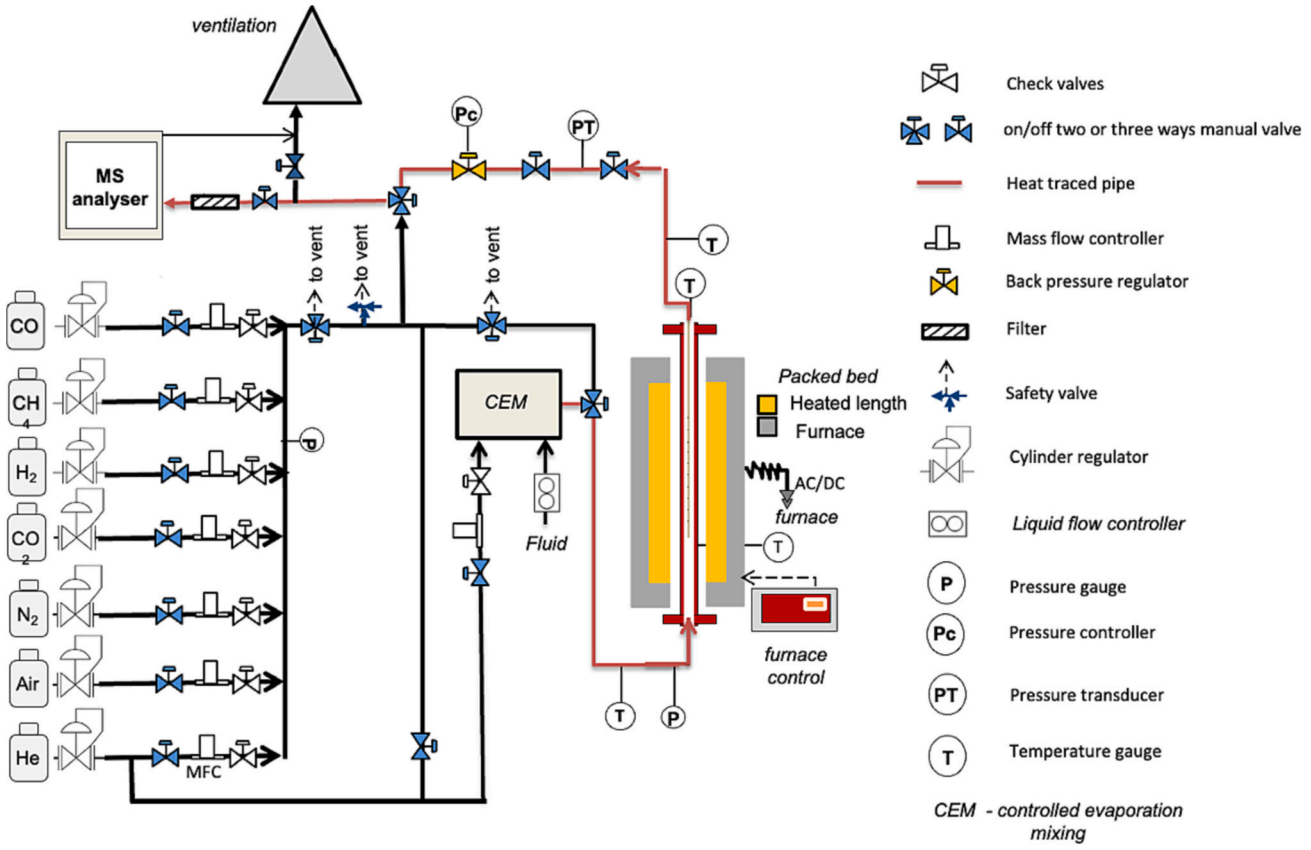

Fig. 3. Schematic of the experimental setup.

Table 1
Experimental conditions for all materials, covering air oxidations, H_2O oxidations, and CO + CO_2 reductions, all at atmospheric pressure.

	LSF-641		Fe2O3-NiO/LSF-641	
Reactions	Temperature (°C)	Flowrate (sccm)	Temperature (°C)	Flowrate (sccm)
Oxidation	600–800	100 Air; 100 He	600–800	100 Air; 100 He
Steam Oxidation	700–900	45 H_2O; 505 He	700–900	45 H_2O; 505 He
Reduction	600–900	100 (CO + CO_2); 100 He	600–900	100 (CO + CO_2); 100 He

recuperated. The behaviour of composite materials was observed by Dueso et al. [25], who underwent TGA testing of several different OCMs composed of LSF-731 and iron oxides. Findings showed that the reactivity of the OCM did not correspond to the summation of both components but rather a synergetic effect resulting in a higher capacity material. Thursfield et al. [26] and Galinsky et al. [23] suggested using perovskites to support metal oxides to increase both kinetics while preserving the OC capacity. Perovskites used in literature include LSF-731 and LSF-821; no composite oxygen carriers operating LSF-641 have been tested [25,27–29]. Preparation methods associated with

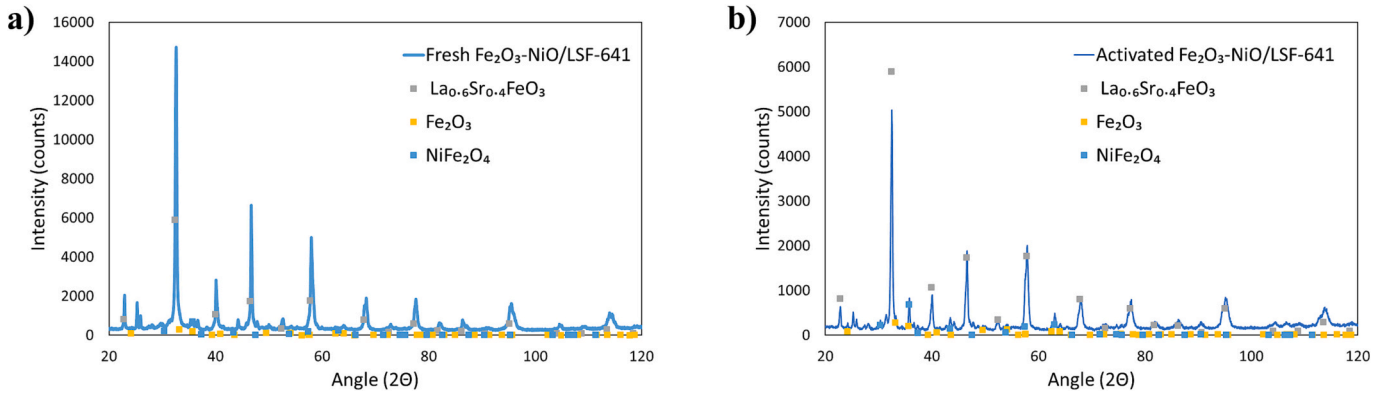

Fig. 4. XRD peak analysis for a) fresh Fe_2O_3-NiO/LSF-641 and b) Fe_2O_3-NiO/LSF-641 after activation.

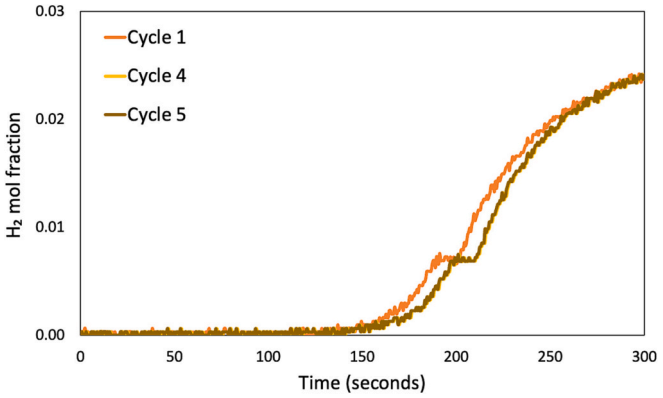

Fig. 5. a) Fe_2O_3-NiO/LSF-641 activation (90% He, 5% H_2, and 5% CO_2).

adding metal oxides onto perovskites include the infiltration method, solid-state synthesis (SSR), and sol-gel method [25,30–33]. No wet impregnation of metal oxides has been done in the literature, an alternative simple preparation method than SSR and sol-gel being more accessible to carry out and less costly.

Further evaluation of the literature on Fe_2O_3 supported by LSF shows high loadings of Fe_2O_3 up to 60 wt% [25,30,33–35], although Fe loadings lead to sintering and, consequently, degradation in H_2 generation [25,36,37]. Suppressing Fe sintering is achievable by the bimetallic Fe—Ni stabilising interactions; however, for composite perovskites, there is little coverage in the literature, with only Lim et al. [31] testing this concept using 300 mg packed bed reactor, using LSF-821 and equimolar amounts of Fe_2O_3 and NiO. The phase transition of Fe_2O_3-NiO to $NiFe_2O_4$ showed that adding NiO increased oxygen-carrying capacity and the particle's catalytic activity and alleviated sintering. Findings still showed that carbon deposition occurred.

This work aims to cover the gap in moving the development of new material towards long-term stability under repeated cycles while tracking the material stability under a more severe environment in terms of gas composition. This work has focused on the testing and comparison of Fe—Ni bimetallic in LSF-641 to assess the stability and resistance towards carbon deposition while keeping high water splitting capacity during pure H_2 generation. The experimental campaign has been carried out using a 2-g packed bed reactor for all OC material formulations. Both fresh and spent materials were characterised to assess the material morphology, changes and behaviour after operation and at different stages to understand the optimal operation and set the process boundaries for subsequent scale-up.

2. Material and methods

Initially, reference material $La_{0.6}Sr_{0.4}FeO_{3-\delta}$ (LSF-641) was synthesised via the Pechini method, where the material was calcinated at 1050 °C, adapted from de Leeuwe et al. [38] and shown in Fig. 2a and Fig. 2b. More details on the preparation method are reported in the Supplementary Information.

The addition of Fe_2O_3 and NiO to LSF-641 was done via the wet impregnation method as 20 wt% Fe_2O_3 and 3$wt_{\%}$ NiO onto LSF-641 synthesised by the above sol-gel Pechini-method. The precursors were γ-Al_2O_3 (Alfa Asear), $FeN_3O_9{\bullet}9H_2O$ (Fischer Scientific), and Ni $(NO_3)_2{\bullet}(H_2O)_6$. All samples are diluted using 50 ml of water and mixed. Once the solution was homogenous, the mixture was dried for 8 h at 120 °C and calcinated for 5 h at 500 °C. Lower calcination temperatures lead to more significant surface areas [35]. The material was crushed to reduce particle size before partitioning using a 300–700 μm sieve.

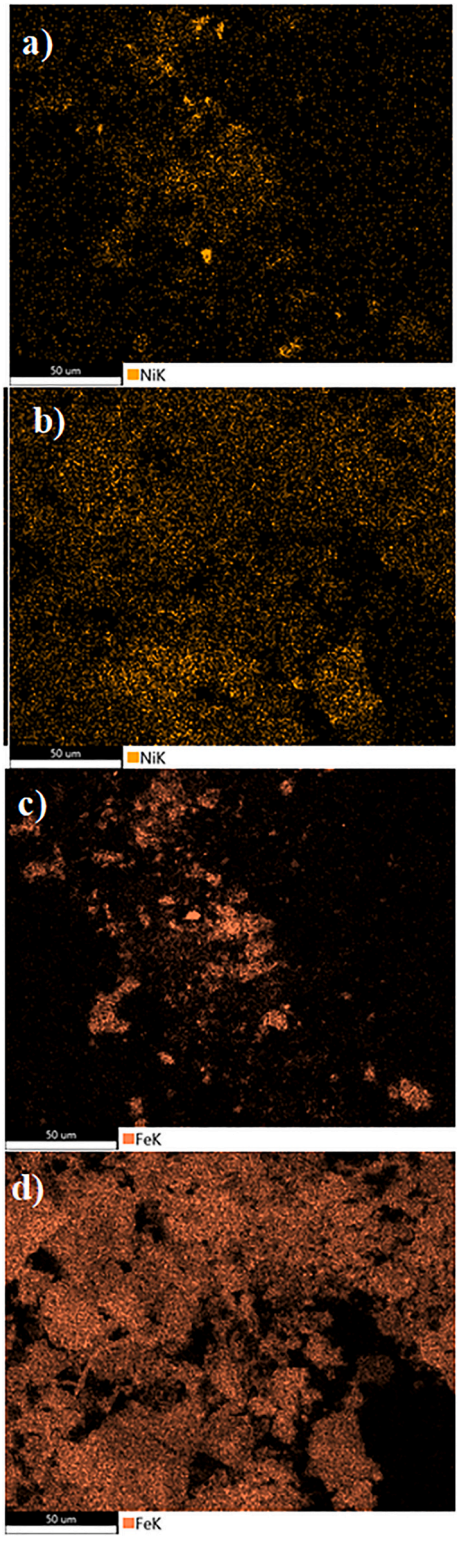

Fig. 6. SEM-EDX elemental mapping of Fe and Ni species of Fe_2O_3-NiO/LSF-641, (a) Ni fresh, (b) Ni after activation, (c) Fe fresh, (d) Fe after activation. Mapping shows a more homogenous metal oxide dispersion, reducing clustering.

2.1. Experimental rig set-up

Experimental work occurred in a rig for testing material and a small-scale reactor (Fig. 3). Seven gases are available (CO, CH_4, H_2, Air, N_2, He, CO_2) and controlled by Bronkhorst flow controllers, and one liquid

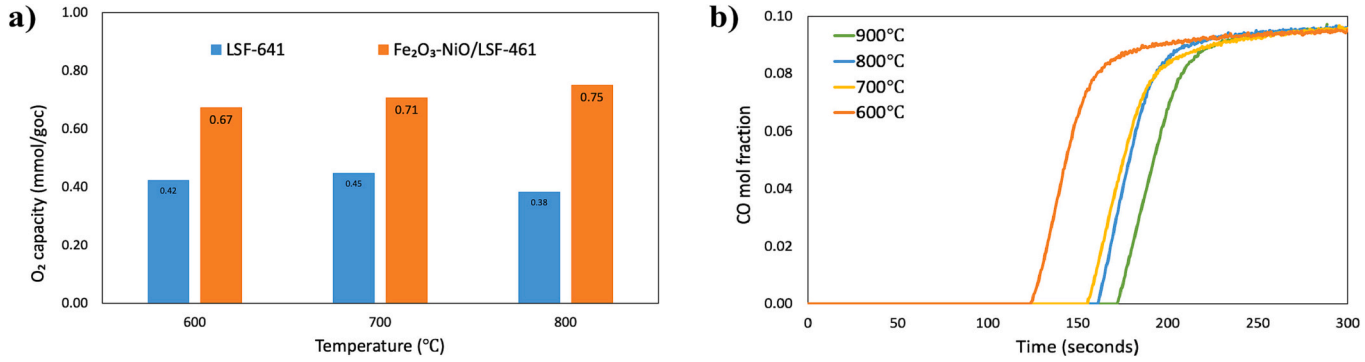

Fig. 7. a) OTC of LSF-641 and Fe_2O_3-NiO/LSF-641 from 600 to 800 °C.b) Temperature varying reduction profile of Fe_2O_3-NiO/LSF-641 from 600 to 900 °C.

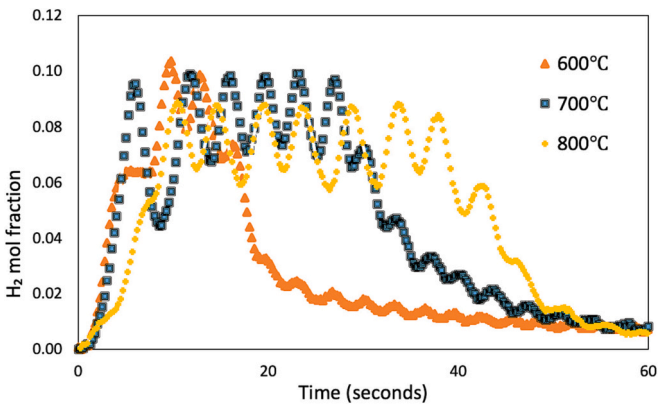

Fig. 8. LSF-641 chemical looping hydrogen experiments using 2 g/min H_2O feed (600–800 °C, 1 atm) Inlet gas: He 91% with H_2O 9%.

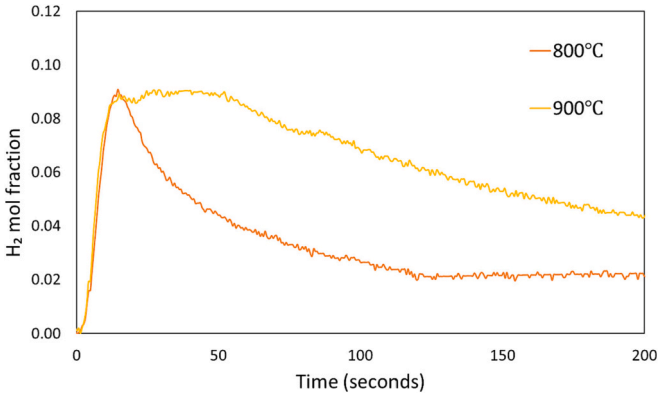

Fig. 9. Fe_2O_3-NiO/LSF-641 steam oxidation experiments using 2 g/min H_2O.

flow controller is used to feed liquid (such as H_2O). The liquid is stored in a pressurised vessel, and the evaporation occurs using Bronkhorst's controlled evaporating mixer (CEM) and heated lines before and after the quartz reactor.

The packed bed reactor was quartz silica (L × OD × WT: 550 × 130 × 2 mm) housed in a Carbolite furnace, with temperature transducers at the reactor inlet, outlet and in contact with the OC. All experiments were conducted at atmospheric pressure with an operating temperature range of 400–900 °C. After the gases were cooled, gas composition measurements were carried out using a HIDEN HPR-20 Mass Spectrometer.

Inert material (quartz wool) at the bottom and top of the bed ensures that the material is held in the middle reactor and that the feed gases are pre-heated and homogenously distributed along the cross-section [39]

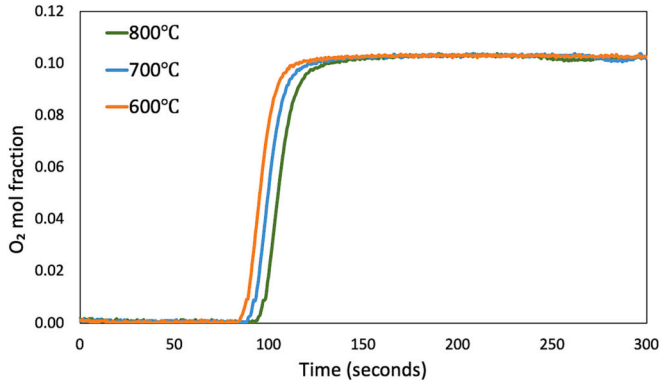

Fig. 10. Oxidation profiles of all Fe_2O_3-NiO/LSF-641.

(shown Fig. 2c). The material is kept at a uniform temperature, 2 g of LSF-641 and LSF-Fe_2O_3-Ni, at a 300–700 μm particle size approximating an 8 cm bed height—the system's control through the LabVIEW® interface.

2.2. Experimental conditions

Experimental conditions are reported in Table 1. Reactions considered are oxidations using air, partial oxidations using H_2O, and reductions using mixtures of CO and CO_2.

3. Results and discussion

3.1. Fresh and activated samples characterisation

X-ray diffraction (XRD) was done using a Bruker D8 Discover GIXRD Autochanger. LSF-641 XRD analysis shows the formation of the compound LSF-641 (results reported in the Supplementary Information). Fe_2O_3-NiO/LSF-641 shows peaks for Fe_2O_3 and LSF-641, with no peaks for NiO (Fig. 4a). The formation of Ni—Fe alloy, $NiFe_2O_4$ can occur when using Fe and Ni [40]; XRD peaks for Fe_2O_3-NiO/LSF-641 do not show formation of the species; this is because the NiO crystalline structure is either too small to be detected by XRD or the NiO is an amorphous phase, coherently with findings in Kang et al. [36] who prepared a similar material with low wt% of NiO. Formation of $NiFe_2O_4$ can occur during redox cycling.

The material is firstly activated via redox cycling using H_2/CO_2/He and diluted air until the breakthrough times after reduction and oxidation are constant from each cycle. This is required for Fe_2O_3-NiO/LSF-641, while LSF-641 had a constant breakthrough and didn't require activation, attributed to the high calcination temperature allowing for a more thermally stable material [24]. XRD analysis after activation of Fe_2O_3-NiO/LSF-641 shows the presence of $NiFe_2O_4$ species (Fig. 4b).

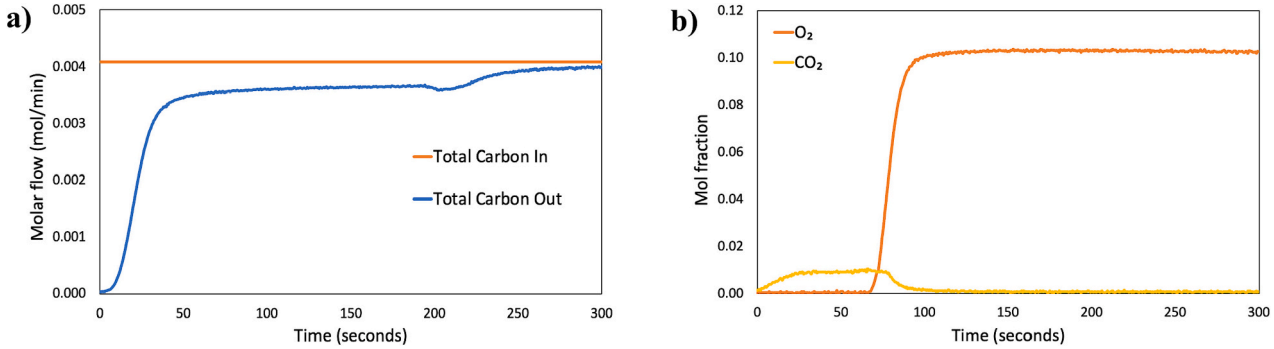

Fig. 11. a) Total molar flow rates of inlet and outlet carbon. b) Air oxidation after reduction using a 4:1 ratio of CO_2 to CO. Oxidation shows the presence of carbon deposition indicated by the release of CO_2.

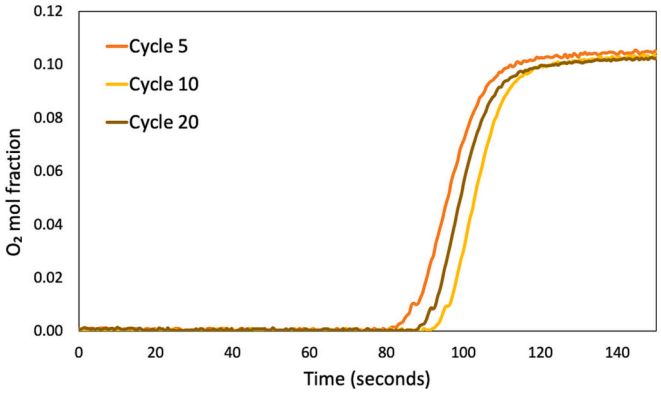

Fig. 12. Fe_2O_3-NiO/LSF-641 capacity change over 20 cycles. Results show an increasing ability from cycle 5 to cycle 10, with a decrease at cycle 20.

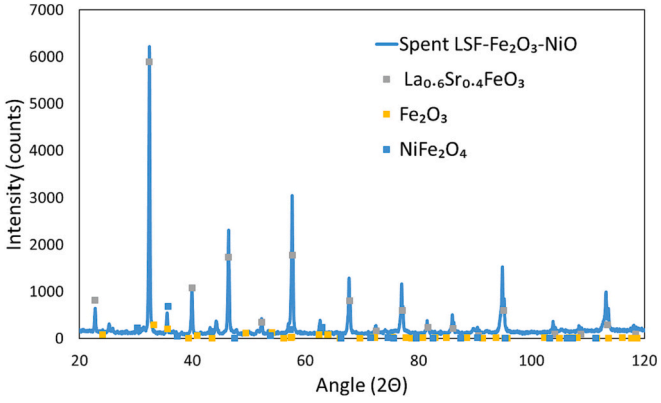

Fig. 13. XRD analysis of spent Fe_2O_3-NiO/LSF-641.

Activation of Fe_2O_3-NiO/LSF-641 (Fig. 5) involved redox cycling for four cycles to achieve a constant breakthrough. During the activation, the OTC increased from 1.76 to 1.80 $mmol_{O_2}/g_{OC}$ under redox conditions. The difference is attributed to the presence of Ni, where Ni has weaker interactions with support materials than Fe, allowing the Ni particles more mobility [14].

FEI Quanta 200 Scanning Electron with Energy Dispersive X-Ray Analysis (SEM-EDX) was used for imagining and elemental mapping of both LSF-641 (refer to SI, Figure S1 and Figure S2) and Fe_2O_3-NiO/LSF-641. LSF-641 shows no difference between pre and post-activation, whilst the Fe_2O_3-NiO/LSF-641 elemental mapping shows that the dispersion of Fe and Ni changes after the material is activated, with previous clusters of Fe and Ni dispersing on the surface of perovskite, providing a more homogenous distribution of Ni and Fe (Fig. 6).

3.2. Reduction

All materials are reduced in a CO-rich gas, to show the effects of temperature on reduction, the oxidation is performed at 700 °C, whilst reduction temperature is varied (Fig. 7). LSF-641 reduction shows variable O_2 non-stoichiometric (Fig. 7a). This is due to the thermal expansion of the perovskite changing the interaction between the A and B site atoms in the lattice, leading to a release of O_2, with higher facilitation of O_2 release at higher temperatures [41]. This leads to 700 °C being the optimum temperature, with the longest breakthrough time of 193 s, with a bed temperature of 800 °C breaking through after 180 s and 900 °C 155 s. The reduction temperature variation trend shown by Fe_2O_3-NiO/LSF-641 (Fig. 7b) is an increasing O_2 capacity, as temperature increases with 900 °C showing optimum O_2 capacity, with a breakthrough time of 175 s. This is because, at higher temperatures, the formed porous Ni layer increases, resulting in Ni circular caps with higher porosity, allowing more gas to access the underlying NiO and furthering the extent of reduction [42,43].

3.3. Steam oxidation

H_2 generation from steam oxidation occurs under the equilibrium oxygen chemical potential of H_2O, which depends on temperature [44], with H_2 production increasing at increased temperature [45]. The results fluctuate due to a pulsing effect of the experimental setup under the presence of water-to-hydrogen, which is received by the gas analyser intermittently. To circumvent this rig limitation, outlet compositions have been integrated and averaged, and the mass balance has been checked for all experiments to avoid amplifying the errors by fluctuations. H_2O reacts with the reduced LSF to produce H_2 (Fig. 8) with H balance satisfied and closed to the extent of a ± 4% error, and at 600 °C H_2 purity of 98% (the rest is H_2O), lasting for 10 s. At 700 °C, H_2 purity decreases to 93%, with the remainder being H_2O for around 30 s, and at 800 °C, H_2 purity drops to 89% for 40 s. The results strongly indicate greater bed utilisation at higher temperatures for H_2 generation despite the decrease in H_2O-to-H_2 conversions. Compared to literature, the steam conversion for LSF-641 is similar, where average steam conversion of 96% are obtained during water splitting [46–48]. The decrease in purity implies a minimal effect on the H_2 purity since after H_2O condensation (ambient temperature) the purity could increase >98%.

In the case of Fe_2O_3-NiO/LSF-641, only the Fe containing species undergo water splitting, Ni-based OC cannot undergo H_2O splitting due to limitations in thermodynamic properties and reaction kinetics [49], rendering the water-splitting reaction unfeasible. The results showed that increased temperature generates more H_2 because the increased Fe content (Fig. 9). At all temperatures, 100% H_2O conversion is achieved in the initial stages before the H_2O breakthrough. At 800 °C, H_2O conversion is 100% for 10 s, increasing to 60 s at 900 °C. At 900 °C, 4.633 $mmol/g_{oc}$ of H_2 were obtained without outfacing deactivation issues via

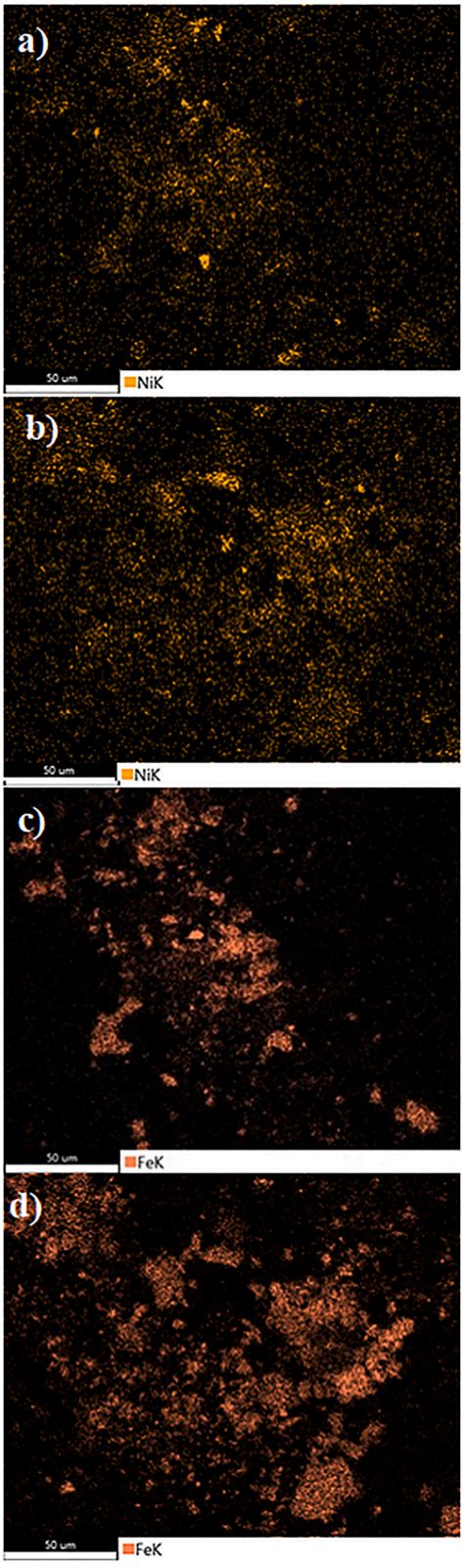

Fig. 14. SEM-EDX elemental mapping of Fe and Ni species of Fe_2O_3-NiO/LSF-641, (a) Ni pre-experimental work, (b) Ni after 20 cycles, (c) Fe pre-experimental work, (d) Fe after 20 cycles.

the formation of metallic Fe [50]. This is approximately 20 more H_2 than the same mass of LSF-641 (0.236 $mmol/g_{oc}$ of H_2 at 700 °C), which is consistent with literature data, there in an increase in H_2 compared 70wt % Fe_2O_3 supported on Al_2O_3 generates 1.2 mmol/goc H_2, and is within the range of other iron composite perovskites, where perovskites such as supported on $Ce_{0.75}Zr_{0.75}O_2$, and $La_{0.8}Sr_{0.2}FeO_3$ are used as supports, H_2 generation ranges from 3.5 to 10 $mmol/g_{oc}$ [50,51].

3.4. Oxidation with air

The effect of temperature (500–700 °C range) during oxidation with air in LSF-641 was carried out starting from the bed fully reduced at 700 °C in presence of CO and then cooled down to ensure that the material was always at the same oxidation state after the reduction (refer to SI, Figure S3). The effect of the temperature is relevant only for the slope during the breakthrough which is higher at higher temperature. Further estimates on the LSF loss of capacity have been recorded in SI (Figure S4) during the pre-heating of the bed under inert gas conditions due to the variable non-stoichiometry of the LSF-641 with temperature [38]. To verify the exact OTC of the material at 800 °C and 900 °C during the reduction and oxidation, the material was heated >800 °C with a constant p_{O_2}. This was verified by monitoring the outlet gas compositions during heat-up under an inert atmosphere. This confirmed that the O_2 released during heating amounted to 0.205 $mmol_{O_2}/g_{oc}$, accounting for 47% of the O_2 uptake during air oxidation, with the material showing an 3.28% weight loss.

In case of Fe_2O_3-NiO/LSF-641, the sensitivity analysis on air oxidation was carried out after reduction with CO/CO_2/He (1/1/2) at 900 °C. Similarly to the previous case, the cooling of the bed was carried out under inert conditions to avoid any change in the initial oxidation state of the materials.

The optimal conditions for air oxidation are at 800 °C, with O_2 breakthrough at 93 s with the uptake of 0.751 $mmol_{O_2}/g_{oc}$ (12.02% material weight loss) (Fig. 10). Breakthroughs at 800 °C, 700 °C and 600 °C occurred at approximately 80–90 s. Breakthrough slope gradients are indicative of the kinetics during oxidation. For Fe_2O_3-NiO/LSF-641, it was found that increasing temperatures lead to faster kinetics, with O_2 diffusion out of the bulk phase occurring quicker with increasing temperature. However, the increase in the slope is almost negligible.

3.5. Carbon deposition

Carbon deposition was identified through the carbon balance due to a decrease in the outlet's total carbon flow (Fig. 11a). CO_2 was produced via air oxidation, where any deposited carbon would be burnt off, appearing as CO_2 in the outlet gas. LSF-641 is highly resistant to carbon deposition and can withstand CO flow with no CO_2 dilution [49]. However, Fe-based OCs require CO_2 dilution to limit carbon deposition, using a 50:50 split of CO to CO_2. Fe_2O_3-NiO/LSF-641 reductions used various CO: CO_2 ratios to determine the material's carbon formation via the Boudouard reaction (Eq. (6)).

$$CO \rightarrow 0.5C + 0.5CO_2 \quad \Delta H_{298} = -86.25\ kJ/mol_{CO} \tag{6}$$

During reduction using a CO_2:CO ratio of 4:1, up to 3% of total feed carbon was deposited (0.161 $mmol/g_{oc}$) (Fig. 11b). Literature studies indicate that carbon deposition doesn't occur until the depletion of active lattice oxygen ($\delta = 3$), which is witnessed with LSF-641, where pure CO flowing with inert He was used to reducing with no signs of carbon deposition [30]. The cause of the carbon deposition is attributed to the high Fe presence on the surface; this is reported by Zong et al. [10], where CO decomposition on the surface Fe sites occurs more readily, with greater Fe concentrations.

3.6. Multiple cycle stability performance

All materials are subject to 70 h of redox cycling. This prolonged cycling showed that LSF is more stable, with only a 1% capacity drop over 20 cycles. This is expected and is corroborated by the literature [24,32,52]. Fe_2O_3-NiO/LSF-641 increases capacity by the 10th cycle of

12.5% (Fig. 12). This increased capacity is due to Fe and Ni dispersion during redox cycling. This leads to a greater porosity, with metal oxide particles moving throughout due to material contraction and expansion, embedding into new positions and leaving previous sites unoccupied, allowing active gas species better access to the bulk of the particle [53]. After 20 cycles, Fe_2O_3-NiO/LSF-641 shows a capacity decrease of 2% (Fig. 12). Whilst an increase from that found for pure LSF-641, a 2% capacity drop is a minor and reasonable trade-off, given the significant increase in H_2 generation.

Characterisation of post-experimental material shows no formation of any new phase, with analysis of XRD peaks for the spent material being the same as the activated material (Fig. 13). Refer to SI, Figure S5 for a comparison of XRD peaks for fresh, activated and spent Fe_2O_3-NiO/LSF-641.

They are comparing pre- and post-experimental elemental mapping of Fe and Ni. No Ni or Fe-dense regions are developed (Fig. 14). Imaging shows a homogenous distribution of Ni and Fe on the surface, with no metal oxide clusters forming as a sign of sintering. The lack of sintering shows an improvement compared to the literature, where Fe_2O_3 composite perovskites suffered from the sintering, whilst in this experiment, the Ni—Fe interaction forming the $NiFe_2O_4$ spinel limits sintering [25]. Thus, the effects of the drop in capacity can be pinpointed and pointed down to carbon deposition. The higher concentration of Fe, as well as the presence of Ni on the surface, increases the risk of carbon deposition [54,55].

4. Conclusion

CLH is a promising technology for pure H_2 generation coupled with inherent CO_2 separation. Fe_2O_3-NiO/LSF-641 was compared with LSF-641. This study showed that Fe_2O_3-composite perovskites, showing that the simple preparation method of wet impregnation, compared to those used in literature, of Fe_2O_3 and NiO improved performance, and with the formation of $NiFe_2O_4$, spinel metal ion sintering was prevented, increasing the O_2 transport capacity and a significant increase in H_2 generation. The material suffered from minor carbon deposition, resulting in a slight capacity decrease of 2% over 20 cycles. This study shows that modifications of LSF-641 via adding bimetallic Fe—Ni particles onto the surface increase H_2 yield. Furthermore, Fe—Ni interaction results show an increase in the catalytic activity and stability of the OC and improve metal nanoparticle dispersion suppressing sintering. Improvements can be made in stopping carbon deposition, where the loading of Ni within the perovskite lattice will be studied to discover the impact of material preparation and the potential for more stable and carbon-resistant OC with greater H_2 production capacity and faster kinetics.

CRediT authorship contribution statement

Adam Zaidi: Data curation, Formal analysis, Investigation, Methodology, Validation, Visualization, Writing – original draft. **Christopher de Leeuwe:** Formal analysis, Investigation, Validation, Visualization, Writing – review & editing. **Vincenzo Spallina:** Conceptualization, Funding acquisition, Project administration, Resources, Supervision, Validation, Writing – review & editing.

Declaration of competing interest

The authors declare that they have no known competing financial interests or personal relationships that could have appeared to influence the work reported in this paper.

Data availability

Data will be made available on request.

Acknowledgement

The authors would like to acknowledge the EU Horizon 2020 research and innovation programme under grant agreement no. 884197 (GLAMOUR project) and the EPSRC BREINSTORM project, EP/S030654/1.

Appendix A. Supplementary data

Supplementary data to this article can be found online at https://doi.org/10.1016/j.powtec.2024.119510.

References

[1] IEA, Chemicals, 2020.
[2] A. Abdalla, M. Mohamedali, N. Mahinpey, Recent progress in the development of synthetic oxygen carriers for chemical looping combustion applications, Catal. Today 407 (2023) 21–51, https://doi.org/10.1016/j.cattod.2022.05.046.
[3] S. Bhavsar, M. Najera, R. Solunke, G. Veser, Chemical looping: to combustion and beyond, Catal. Today 228 (2014) 96–105, https://doi.org/10.1016/j.cattod.2013.12.025.
[4] B. Dou, K. Wu, H. Zhang, B. Chen, H. Chen, Y. Xu, Sorption-enhanced chemical looping steam reforming of glycerol with CO2 in-situ capture and utilization, Chem. Eng. J. 452 (2023) 139703, https://doi.org/10.1016/j.cej.2022.139703.
[5] B. Dou, L. Zhao, H. Zhang, K. Wu, H. Zhang, Renewable hydrogen production from chemical looping steam reforming of biodiesel byproduct glycerol by mesoporous oxygen carriers, Chem. Eng. J. 416 (2021) 127612, https://doi.org/10.1016/j.cej.2020.127612.
[6] G. Voitic, S. Nestl, K. Malli, J. Wagner, B. Bitschnau, F.A. Mautner, V. Hacker, High purity pressurised hydrogen production from syngas by the steam-iron process, RSC Adv. 6 (2016), https://doi.org/10.1039/c6ra06134f.
[7] NIST, NIST Chemistry WebBook, 2022.
[8] J. Adánez, L.F. De Diego, F. García-Labiano, P. Gayán, A. Abad, J.M. Palacios, Selection of oxygen carriers for chemical-looping combustion, Energy Fuel 18 (2004), https://doi.org/10.1021/ef0301452.
[9] S. Ma, S. Chen, A. Soomro, W. Xiang, Effects of supports on hydrogen production and carbon deposition of Fe-based oxygen carriers in chemical looping hydrogen generation, Int. J. Hydrog. Energy 42 (2017), https://doi.org/10.1016/j.ijhydene.2017.02.132.
[10] T. Zong, L. Li, Y. Han, C. Wang, Y. Kang, M. Tian, C. Huang, X. Wang, Influence of the encapsulation degree of Fe0 active sites on performance of garnets for chemical looping partial oxidation of CH4, Appl. Catal. B 312 (2022) 121421, https://doi.org/10.1016/j.apcatb.2022.121421.
[11] A. Abdalla, M. Mohamedali, N. Mahinpey, Recent progress in the development of synthetic oxygen carriers for chemical looping combustion applications, Catal. Today 407 (2023) 21–51, https://doi.org/10.1016/j.cattod.2022.05.046.
[12] Y. Lin, Z. Zhang, H. Wang, S. Fang, Z. Huang, T. Chen, G. Wei, K. Zhao, Z. Zhao, J. Wu, Y. Fang, H. Li, An evaluation of the reactivity of synthetic Fe-Ni oxygen carriers: CO oxidation, H2O reforming, and toluene cracking, Energy Convers. Manag. 240 (2021) 114263, https://doi.org/10.1016/j.enconman.2021.114263.
[13] S. Bhavsar, G. Veser, Bimetallic Fe–Ni oxygen carriers for chemical looping combustion, Ind. Eng. Chem. Res. 52 (2013) 15342–15352, https://doi.org/10.1021/ie400612g.
[14] M.A. Pans, P. Gayán, A. Abad, F. García-Labiano, L.F. De Diego, J. Adánez, Use of chemically and physically mixed iron and nickel oxides as oxygen carriers for gas combustion in a CLC process, Fuel Process. Technol. 115 (2013), https://doi.org/10.1016/j.fuproc.2013.05.013.
[15] X. Zhu, Q. Imtiaz, F. Donat, C.R. Müller, F. Li, Chemical looping beyond combustion-a perspective, Energy Environ. Sci. 13 (2020), https://doi.org/10.1039/c9ee03793d.
[16] J. Hu, V.V. Galvita, H. Poelman, G.B. Marin, Advanced chemical looping materials for CO2 utilization: a review, Materials. 11 (2018), https://doi.org/10.3390/ma11071187.
[17] Y. Wang, Y. Zheng, Y. Wang, H. Wang, X. Zhu, Y. Wei, Y. Wang, L. Jiang, Z. Yang, K. Li, Evaluation of Fe substitution in perovskite LaMnO3 for the production of high purity syngas and hydrogen, J. Power Sources 449 (2020) 227505, https://doi.org/10.1016/j.jpowsour.2019.227505.
[18] D. Sastre, P. Pizarro, J.M. Coronado, Effect of low-loading of Ni on the activity of La0.9Sr0.1FeO3 perovskites for chemical looping dry reforming of methane, Catal. Today 423 (2023) 114289, https://doi.org/10.1016/j.cattod.2023.114289.
[19] C. de Leeuwe, W. Hu, J. Evans, M. von Stosch, I.S. Metcalfe, Production of high purity H2 through chemical-looping water–gas shift at reforming temperatures – the importance of non-stoichiometric oxygen carriers, Chem. Eng. J. 423 (2021), https://doi.org/10.1016/j.cej.2021.130174.
[20] Q. Chen, S. Hu, Q. Xu, S. Su, Y. Wang, K. Xu, L. He, J. Xiang, Steam synergic effect on oxygen carrier performance and WGS promotion ability of iron-oxides, Energy. 215 (2021), https://doi.org/10.1016/j.energy.2020.119117.
[21] S. Das, A. Biswas, C.S. Tiwary, M. Paliwal, Hydrogen production using chemical looping technology: a review with emphasis on H2 yield of various oxygen carriers, Int. J. Hydrog. Energy 47 (2022) 28322–28352, https://doi.org/10.1016/j.ijhydene.2022.06.170.

[22] M. Kuhn, S. Hashimoto, K. Sato, K. Yashiro, J. Mizusaki, Oxygen nonstoichiometry, thermo-chemical stability and lattice expansion of La0.6Sr0.4FeO3−δ, Solid State Ionics 195 (2011) 7–15, https://doi.org/10.1016/j.ssi.2011.05.013.
[23] N.L. Galinsky, Y. Huang, A. Shafiefarhood, F. Li, Iron oxide with facilitated O 2– transport for facile fuel oxidation and CO 2 capture in a chemical looping scheme, ACS Sustain. Chem. Eng. 1 (2013) 364–373, https://doi.org/10.1021/sc300177j.
[24] F. He, F. Li, Perovskite promoted iron oxide for hybrid water-splitting and syngas generation with exceptional conversion, Energy Environ. Sci. 8 (2015), https://doi.org/10.1039/c4ee03431g.
[25] C. Dueso, C. Thompson, I. Metcalfe, High-stability, high-capacity oxygen carriers: Iron oxide-perovskite composite materials for hydrogen production by chemical looping, Appl. Energy 157 (2015) 382–390, https://doi.org/10.1016/j.apenergy.2015.05.062.
[26] A. Thursfield, A. Murugan, R. Franca, I.S. Metcalfe, Chemical looping and oxygen permeable ceramic membranes for hydrogen production – a review, Energy Environ. Sci. 5 (2012), https://doi.org/10.1039/c2ee03470k.
[27] H. Ohayon Dahan, G. Sror, M.V. Landau, M. Herskowitz, Chemical looping reaction of methane with oxygen from La0.8Sr0.2FeO3-δ and La0.8Sr0.2FeO3-δ -Fe2O3 systems to syngas, discover, Chem. Eng. 2 (2022) 3, https://doi.org/10.1007/s43938-022-00010-5.
[28] H.S. Lim, D. Kang, J.W. Lee, Phase transition of Fe2O3–NiO to NiFe2O4 in perovskite catalytic particles for enhanced methane chemical looping reforming-decomposition with CO2 conversion, Appl. Catal. B 202 (2017) 175–183, https://doi.org/10.1016/j.apcatb.2016.09.020.
[29] H. Ohayon Dahan, M.V. Landau, R. Vidruk Nehemya, E. Edri, M. Herskowitz, C. Ruan, F. Li, Core-Shell Fe2O3@La1−xSrxFeO3−δ material for catalytic oxidations: coverage of Iron oxide Core, oxygen storage capacity and reactivity of surface oxygens, Materials. 14 (2021) 7355, https://doi.org/10.3390/ma14237355.
[30] A. Shafiefarhood, N. Galinsky, Y. Huang, Y. Chen, F. Li, Fe 2 O 3 @La x Sr 1− x FeO 3 core-shell redox catalyst for methane partial oxidation, ChemCatChem. 6 (2014) 790–799, https://doi.org/10.1002/cctc.201301104.
[31] H.S. Lim, D. Kang, J.W. Lee, Phase transition of Fe2O3–NiO to NiFe2O4 in perovskite catalytic particles for enhanced methane chemical looping reforming-decomposition with CO2 conversion, Appl. Catal. B 202 (2017) 175–183, https://doi.org/10.1016/j.apcatb.2016.09.020.
[32] H. Ohayon Dahan, G. Sror, M.V. Landau, M. Herskowitz, Chemical looping reaction of methane with oxygen from La0.8Sr0.2FeO3-δ and La0.8Sr0.2FeO3-δ -Fe2O3 systems to syngas, discover, Chem. Eng. 2 (2022) 3, https://doi.org/10.1007/s43938-022-00010-5.
[33] H. Ohayon Dahan, M.V. Landau, R. Vidruk Nehemya, E. Edri, M. Herskowitz, C. Ruan, F. Li, Core-Shell Fe2O3@La1−xSrxFeO3−δ material for catalytic oxidations: coverage of Iron oxide Core, oxygen storage capacity and reactivity of surface oxygens, Materials. 14 (2021) 7355, https://doi.org/10.3390/ma14237355.
[34] F. He, J. Trainham, G. Parsons, J.S. Newman, F. Li, A hybrid solar-redox scheme for liquid fuel and hydrogen coproduction, Energy Environ. Sci. 7 (2014) 2033–2042, https://doi.org/10.1039/C4EE00038B.
[35] Y. Chen, N. Galinsky, Z. Wang, F. Li, Investigation of perovskite supported composite oxides for chemical looping conversion of syngas, Fuel. 134 (2014) 521–530, https://doi.org/10.1016/j.fuel.2014.06.017.
[36] A. Shafiefarhood, J.C. Hamill, L.M. Neal, F. Li, Methane partial oxidation using FeOx@La0.8Sr0.2FeO3-δ core-shell catalyst-transient pulse studies, Phys. Chem. Chem. Phys. 17 (2015), https://doi.org/10.1039/c5cp05583k.
[37] F. He, J. Trainham, G. Parsons, J.S. Newman, F. Li, A hybrid solar-redox scheme for liquid fuel and hydrogen coproduction, Energy Environ. Sci. 7 (2014) 2033–2042, https://doi.org/10.1039/C4EE00038B.
[38] C. de Leeuwe, W. Hu, D. Neagu, E.I. Papaioannou, S. Pramana, B. Ray, J.S. O. Evans, I.S. Metcalfe, Revisiting the thermal and chemical expansion and stability of La0.6Sr0.4FeO3−, J. Solid State Chem. 293 (2021) https://doi.org/10.1016/j.jssc.2020.121838.
[39] P. Alexandros Argyris, C. de Leeuwe, S.Z. Abbas, A. Amieiro, S. Poultson, D. Wails, V. Spallina, Chemical looping reforming for syngas generation at real process conditions in packed bed reactors: an experimental demonstration, Chem. Eng. J. 435 (2022) 134883, https://doi.org/10.1016/j.cej.2022.134883.
[40] Y.L. Kuo, W.C. Huang, W.M. Hsu, Y.H. Tseng, Y. Ku, Use of spinel nickel aluminium ferrite as self-supported oxygen carrier for chemical looping hydrogen generation process, Aerosol Air Qual. Res. 15 (2015), https://doi.org/10.4209/aaqr.2015.05.0300.
[41] T. Götsch, L. Schlicker, M.F. Bekheet, A. Doran, M. Grünbacher, C. Praty, M. Tada, H. Matsui, N. Ishiguro, A. Gurlo, B. Klötzer, S. Penner, Structural investigations of La 0.6 Sr 0.4 FeO 3−δ under reducing conditions: kinetic and thermodynamic limitations for phase transformations and iron exsolution phenomena, RSC Adv. 8 (2018) 3120–3131, https://doi.org/10.1039/C7RA12309D.
[42] A. Abad, F. García-Labiano, L.F. de Diego, P. Gayán, J. Adánez, Reduction kinetics of Cu-, Ni-, and Fe-based oxygen carriers using syngas (CO + H 2) for chemical-looping combustion, Energy Fuel 21 (2007) 1843–1853, https://doi.org/10.1021/ef070025k.
[43] J. Chen, P.C. Hayes, Mechanisms and kinetics of reduction of solid NiO in CO/CO2 and CO/Ar gas mixtures, Metall. Mater. Trans. B Process Metall. Mater. Process. Sci. 50 (2019) 2623–2635, https://doi.org/10.1007/s11663-019-01662-5.
[44] David John Young, High Temperature Oxidation and Corrosion of Metals, 2nd ed., Elsevier, 2016.
[45] V. Spallina, F. Gallucci, M.C. Romano, M. Van Sint Annaland, Pre-combustion packed bed chemical looping (PCCL) technology for efficient H2-rich gas production processes, Chem. Eng. J. 294 (2016) 478–494, https://doi.org/10.1016/j.cej.2016.03.011.
[46] L. Zhao, B. Dou, H. Zhang, Z. Wang, Oxygen carriers for chemical-looping water splitting to hydrogen production: a critical review, Carbon Capture Sci. Technol. 1 (2021) 100006, https://doi.org/10.1016/j.ccst.2021.100006.
[47] G. Voitic, V. Hacker, Recent advancements in chemical looping water splitting for the production of hydrogen, RSC Adv. 6 (2016) 98267–98296, https://doi.org/10.1039/C6RA21180A.
[48] A. Murugan, Iron-Containing Perovskite Materials for Stable Hydrogen Production by Chemical Looping Water Splitting, 2012.
[49] L. Zhao, B. Dou, H. Zhang, Z. Wang, Oxygen carriers for chemical-looping water splitting to hydrogen production: a critical review, Carbon Capture Sci. Technol. 1 (2021) 100006, https://doi.org/10.1016/j.ccst.2021.100006.
[50] S. Das, A. Biswas, C.S. Tiwary, M. Paliwal, Hydrogen production using chemical looping technology: a review with emphasis on H2 yield of various oxygen carriers, Int. J. Hydrog. Energy 47 (2022) 28322–28352, https://doi.org/10.1016/j.ijhydene.2022.06.170.
[51] F. He, F. Li, Perovskite promoted iron oxide for hybrid water-splitting and syngas generation with exceptional conversion, Energy Environ. Sci. 8 (2015), https://doi.org/10.1039/c4ee03431g.
[52] U.F. Vogt, J. Sfeir, J. Richter, C. Soltmann, P. Holtappels, B-site substituted lanthanum strontium ferrites as electrode materials for electrochemical applications, pure and applied, Chemistry. 80 (2008) 2543–2552, https://doi.org/10.1351/pac200880112543.
[53] A.J. Carrillo, J.M. Serra, Exploring the stability of Fe–Ni alloy nanoparticles Exsolved from double-layered perovskites for dry reforming of methane, Catalysts. 11 (2021) 741, https://doi.org/10.3390/catal11060741.
[54] H. You, Y. Yuan, J. Li, L.R. Sandoval, A multi-scale model for CO2 capture: a nickel-based oxygen carrier in chemical-looping combustion, IFAC-PapersOnLine. 51 (2018), https://doi.org/10.1016/j.ifacol.2018.09.264.
[55] R. Villa, C. Cristiani, G. Groppi, L. Lietti, P. Forzatti, U. Cornaro, S. Rossini, Ni based mixed oxide materials for CH4 oxidation under redox cycle conditions, J. Mol. Catal. A Chem. 204–205 (2003), https://doi.org/10.1016/S1381-1169(03)00346-7.